Ag^+ diffusion within the rock-salt structured superionic conductor $Ag_4Sn_3S_8$

2005 J. Phys.: Condens. Matter 17 1067

(http://iopscience.iop.org/0953-8984/17/7/002)

INSTITUTE OF PHYSICS PUBLISHING JOURNAL OF PHYSICS: CONDENSED MATTER

J. Phys.: Condens. Matter **17** (2005) 1067–1084 doi:10.1088/0953-8984/17/7/002

Ag^+ diffusion within the rock-salt structured superionic conductor $Ag_4Sn_3S_8$

S Hull[1,3], P Berastegui[2] and A Grippa[2]

[1] The ISIS Facility, Rutherford Appleton Laboratory, Chilton, Didcot, Oxfordshire OX11 0QX, UK
[2] Department of Inorganic Chemistry, Arrhenius Laboratory, Stockholm University, S-106 91 Stockholm, Sweden

E-mail: s.hull@rl.ac.uk

Received 2 November 2004, in final form 10 January 2005
Published 4 February 2005
Online at stacks.iop.org/JPhysCM/17/1067

Abstract

The temperature dependence of the crystal structure of the compound $Ag_4Sn_3S_8$ and its Ag^+ ionic conduction mechanisms have been investigated using impedance spectroscopy measurements, powder neutron diffraction studies and computer simulations. Under ambient conditions, $Ag_4Sn_3S_8$ adopts a cubic structure in space group $P4_132$ with $a = 10.808\,98(7)$ Å and $Z = 4$. The S^{2-} form a slightly distorted fcc structured anion sublattice with the $16 \times Ag^+$ and $12 \times Sn^{4+}$ arranged in an ordered manner over the 32 available octahedrally coordinated cavities. As a result, the crystal structure of $Ag_4Sn_3S_8$ can be described as a slightly deformed, cation deficient rock-salt arrangement. Highly anisotropic thermal vibrations of the Ag^+ are observed, especially at elevated temperatures. Above ≈500 K, analysis of the powder neutron diffraction data provides evidence for limited thermally induced cation disorder, associated with an increasing occupancy of the empty octahedrally coordinated positions. This behaviour is successfully reproduced within molecular dynamics simulations, which identify two different Ag^+ diffusion mechanisms which occur via a subset of the tetrahedrally coordinated interstices. A brief discussion of the wider issue of superionic behaviour within rock-salt structured compounds is also given.

1. Introduction

Halide and chalcogenide compounds containing monovalent silver continue to attract significant interest in the study of structure–property relationships within superionic conductors (for a recent review, see [1]). Whilst their commercial application within solid state devices is limited by several factors, including the high cost of silver, the impressive values of ionic

[3] Author to whom any correspondence should be addressed.

conductivity shown at relatively modest temperatures makes them ideal model systems in which to probe the ionic conduction processes and the factors which promote extensive ionic disorder within solids.

The superionic phases observed within the Ag^+ halides and chalcogenides (and their Cu^+ analogues) are essentially characterized by rapid jump diffusion of the cations between the interstices formed by a sublattice of immobile anions. The latter can be body centred cubic (bcc), face centred cubic (fcc) or hexagonal close packed (hcp) (see [1, 2], and references therein). In general, the ionic conductivity of bcc structured superionic phases is higher than that of fcc and hcp structured ones, as illustrated by the binary CuX (X = Cl, Br and I) [3] and Ag_2X (X = S and Te) [4] systems and by several ternary derivatives of AgI [5–8]. This observation is a consequence of the cations' preference for hops between the tetrahedrally coordinated (T) interstices within the anion sublattice and the greater number of these cavities within the bcc case (six per anion) than the other two lattices (two per anion) [1, 2].

Intuitively, the same arguments should apply if cation diffusion occurs between the octahedrally coordinated (O) voids, because the bcc sublattice also possesses a greater number of these cavities (three per anion rather than one). However, superionic phases characterized by Ag^+ diffusion between the O sites are rather rare. One example is the high pressure rock-salt structured form of AgI, which undergoes a continuous transition to a superionic phase on heating [9], though the onset of cation disorder at temperatures in excess of ∼500 K is characterized by an increased occupancy of the tetrahedral T positions [10, 11]. In this context, and as part of a comprehensive study of ternary derivatives of the binary Ag^+ halide and chalcogenide systems (see [5–8, 12, 13]), our attention has recently been focused on the structure–property relationships within superionic ternary derivatives of the Ag^+ chalcogenides Ag_2S, Ag_2Se and Ag_2Te.

In general, silver chalcogenide based compounds have been less widely studied than their halide counterparts, being more difficult to synthesize in stoichiometric form and often showing a significant electronic contribution to the measured conductivity. Nevertheless, two interesting families of compounds have been identified. Both are based on Ag_2S and can be given the general formulae $Ag_{12-n}M^{n+}S_6$ (M = Ta^{5+}, Nb^{5+}, Ti^{4+}, Ga^{3+} and Al^{3+}) [14–18] and $Ag_4M_3^{4+}S_8$ (M = Sn^{4+}, Zr^{4+} and Hf^{4+}) [19, 20]. Of the latter compounds, $Ag_4Sn_3S_8$ was originally identified within the Ag_2S–SnS_2 phase diagram by Moh and Klein in 1977, together with the compounds Ag_8SnS_6 and Ag_2SnS_3 [21].

X-ray diffraction studies indicated that the crystal structure of $Ag_4Sn_3S_8$ comprises a cubic unit cell with $a = 10.795$ Å, $Z = 4$ and probable space groups $P4_132$ or $P4_332$ [22]. The former was favoured by a subsequent study of a compound of stoichiometry $Ag_{3.8}Sn_3S_8$ by Amiel *et al* [19], who also showed that the structure contained a distorted fcc sublattice of S^{2-}. The Sn^{4+} were located within octahedral cavities and the Ag^+ distributed over three crystallographic sites, two of which were partially occupied. The temperature dependence of the ionic conductivity and structural properties of $Ag_4Sn_3S_8$ are addressed in this paper, using a combination of impedance spectroscopy, powder neutron diffraction and computer simulation methods.

2. Experimental and simulation methods

The sample of $Ag_4Sn_3S_8$ was prepared by solid state synthesis. Stoichiometric amounts of Ag_2S, Sn and S were used as starting materials, with a small excess of sulfur. The mixture was then ground in an agate mortar and pressed into pellets, which were placed in a quartz ampoule which was then evacuated. The sample was annealed for one week at 875 K, cooled by switching off the furnace, reground and annealed at 675 K for five days.

Two-terminal measurements of the conductivity were performed using a pelleted sample of 8 mm diameter and 3 mm length. This was held between two spring loaded platinum discs inside a ceramic cell which is inserted into the hot-zone of a horizontal tube furnace. Complex impedance measurements were performed every 10 K after allowing the temperature to equilibrate. The maximum temperature used was 563 K. A Solartron 1260 Frequency Response Analyser determined the conventional Z–Z' Bode plot over the frequency range from 100 Hz to 6 MHz. All measurements were performed under flowing argon gas.

The neutron diffraction experiments were performed on the Polaris powder diffractometer at the ISIS facility, UK [23], with the sample encapsulated inside a thin walled vanadium can of 6 mm diameter and 17 mm height. High temperature measurements used a special furnace designed for neutron diffraction experiments and constructed using a vanadium foil resistive heating element and heat shields. Diffraction data were collected using the backscattering detector bank which covers the scattering angles $135° < \pm 2\theta < 160°$ and provides data over the d-spacing range $0.5 < d$ (Å) < 3.2 with an essentially constant resolution of $\Delta d/d \sim 5 \times 10^{-3}$. Data were collected for around 8 h under ambient conditions and at the highest temperature measured (570(2) K) in order to determine full structural details, with additional data collections of approximately 2 h duration performed in steps of ≈25 K to probe the evolution with temperature. Whilst $Ag_4Sn_3S_8$ is reported to decompose at a temperature in excess of 900 K [22], measurements were restricted to below 600 K to avoid loss of sulfur and the associated reduction of Sn^{4+} to Sn^{2+}.

Rietveld profile refinements of the powder diffraction data were performed using the program TF12LS [24], which is based on the Cambridge Crystallographic Subroutine Library [25]. The quality of the fits was assessed using the usual profile (P), weighted profile (WP) and expected weighted profile (EXP) R-factors[4]. Additional information concerning the locations of the disordered Ag^+ ions was provided by maximum entropy analysis of the diffraction data based on the MemSys package (Maximum Entropy Data Consultants Ltd, Cambridge, UK) (for details, see [27]). The ability of this technique to probe the densities of mobile ions within ionically conducting phases has recently been demonstrated for the Ag^+ conductors $RbAg_4I_5$ [12] and Ag_2S [28].

Several molecular dynamics (MD) simulations of the superionic properties of binary compounds such as AgI and Ag_2S have been reported (see, for example, [29, 30] and [31, 32], respectively). Whilst the potential adopted in this work was originally developed in the mid-1980s, it remains the most appropriate for studies of Ag^+ containing compounds. This has been demonstrated by its successful use to probe, for example, the nature of the $\alpha \leftrightarrow \beta$ transition in AgI [30, 33–35], the pressure–temperature phase diagram of AgI [36, 37], the origin of the diffuse neutron and x-ray scattering within α-Ag_2S [31, 32] and the Ag^+ diffusion processes within the solid and liquid phases of the ternary compound Ag_3SI [38]. The general form for the potential between ions i and j is given by

$$V_{ij}(r_{ij}) = \frac{A_{ij}(r_i + r_j)^{n_{ij}}}{r_{ij}^{n_{ij}}} + \frac{Z_i Z_j e^2}{r_{ij}} - \frac{1}{2}(\alpha_i Z_j^2 + \alpha_j Z_i^2)\frac{e^2}{r_{ij}^4} - \frac{W_{ij}}{r_{ij}^6},$$

where A_{ij} is the short range repulsive strength, r_i and r_j are the ionic radii, Z_i and Z_j are the ionic charges (which typically are lower than their formal values), α_i and α_j are the electronic

[4] The R-factors are given by $R_P^2 = \sum_{N_D}(I_{obs} - I_{calc})^2 / \sum_{N_D}(I_{obs})^2$, $R_{WP}^2 = \sum_{N_D} \frac{(I_{obs}-I_{calc})^2}{(\sigma I_{obs})^2} / \sum_{N_D} \frac{(I_{obs})^2}{(\sigma I_{obs})^2}$ and $R_{EXP}^2 = (N_D - N_V) / \sum_{N_D} \frac{(I_{obs})^2}{(\sigma I_{obs})^2}$ [26], where the summations are made over the N_D data points used in the fit. I_{obs} and I_{calc} are the observed and calculated intensities, respectively, and σI_{obs} is the estimated standard deviation on I_{obs} derived from the counting statistics. N_V is the number of fitted variables and N_P is the number of Bragg peaks within the fitted data range.

polarizabilities and W_{ij} are the coefficients of the van der Waals interaction. Following the previously published simulations of Ag_2S [31, 32], we neglect the last term (i.e. $W_{ij} = W = 0$) and take a single value for the different n_{ij} ($n = n_{ij} = 7$) and A_{ij} coefficients. The latter's value of $A = A_{ij} = 0.020$ differs slightly from that used for Ag_2S ($A = A_{ij} = 0.015$ [31]) and was chosen to reproduce the experimentally determined density of $Ag_4Sn_3S_8$ at ambient temperature. The properties of the Ag^+ and S^{2-} ions are given as $r_{Ag^+} = 0.61$ Å, $r_{S^{2-}} = 2.10$ Å, $Z_{Ag^+} = +0.45$, $Z_{S^{2-}} = -0.90$, $\alpha_{Ag^+} = 0$ and $\alpha_{S^{2-}} = 6.52$ Å^3 [31]. Charge neutrality requires $Z_{Sn^{4+}} = 4 \times Z_{Ag^+} = +1.80$, whilst the two remaining parameters are given values $r_{Sn^{4+}} = 0.69$ Å [39] and $\alpha_{Sn^{4+}} = 0$.

Simulations were performed at constant (zero) pressure using $2 \times 2 \times 2$ unit cells of $Ag_4Sn_3S_8$, containing a total of $128 \times Ag^+$, $96 \times Sn^{4+}$ and $256 \times S^{2-}$. The initial simulations at 300 K were started using the ionic locations determined experimentally (see section 3.3) and the final configuration used as the input to subsequent simulations at 350 and 250 K. In this iterative manner a total of 20 temperatures were investigated over the range from 50 to 1000 K. Melting of the simulated configuration occurred at 1000 K. The simulations were performed in 1000 000 intervals over a time period of ~600 ps, with the initial 100 ps portion ignored due to equilibration effects and the remaining data used for analysis of the ionic motions. The mean distribution of ions within the unit cell was determined by averaging over time t and over all the unit cells in the simulation box. The diffusion coefficient of Ag^+, D_{Ag^+}, was obtained from the slope of the mean squared displacement at long times, i.e. $D_{Ag^+} = \lim_{t\to\infty} \frac{1}{6N_{Ag^+}t} \langle \sum_{j=1}^{N_{Ag^+}} [r_j(t) - r_j(0)]^2 \rangle$. The ionic conductivity, σ_i, is then be estimated using the expression $\sigma_{Ag^+} = c_{Ag^+} D_{Ag^+} Z^2_{Ag^+}/kT$, where c_{Ag^+} is the concentration of Ag^+.

3. Results

3.1. Conductivity measurements

The measured conductivity of $Ag_4Sn_3S_8$ illustrated in figure 1 is in broad agreement with the values published by Amiel *et al* [19], though we find no evidence for the anomalous behaviour of the conductivity observed at temperatures around 430 K in their work. The data presented in figure 1 represent the *total* conductivity of the sample and, since $Ag_4Sn_3S_8$ has been shown to possess significant electronic conductivity [19], a degree of caution must be used when making comparisons with the ionic conductivity data provided by the computer simulations. In principle, the electronic and ionic components of the conductivity can be separated experimentally using an 'electron blocking' layer of a predominantly Ag^+-ion conductor (such as $RbAg_4I_5$ [19]). However, this procedure has not been performed in this work, since our interest lies principally in the evolution of the conductivity with temperature rather than its absolute value. Indeed, the ionic conductivity derived from the simulations using the expressions given at the end of section 2 is itself a rather crude estimate, because it ignores effects of correlations between diffusing ions (which are often significant within Ag^+ conductors; see [40]) and depends upon the choice of the Ag^+ ions' charge (either the 'formal' $Z_{Ag^+} = +1.0$ or the value $Z_{Ag^+} = +0.45$ which is used within the simulations [29]).

3.2. Description of the fcc structured sublattice

Before describing the results of the powder neutron diffraction studies of the crystal structure of $Ag_4Sn_3S_8$ it is instructive to consider the crystallographic properties of the fcc sublattice

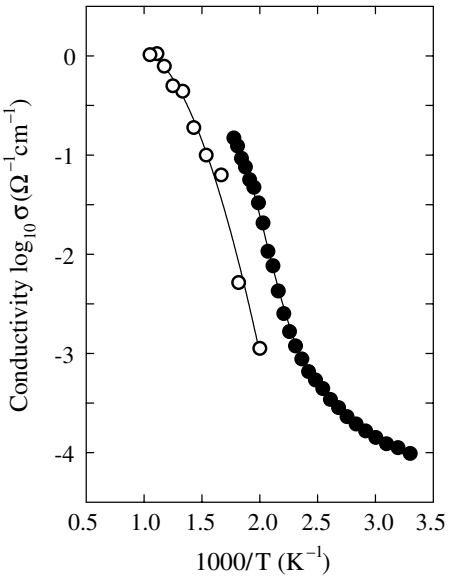

Figure 1. The temperature variation of the measured total conductivity of $Ag_4Sn_3S_8$, plotted as $\log_{10}\sigma$ versus $1000/T$ and shown by the filled symbols (●). The values for the ionic conductivity provided by the computer simulations are shown as open symbols (○). At temperatures below 500 K the simulations give no conductivity information because no Ag^+ diffusion occurs within the timescale of the calculations. The solid curves are guides to the eye.

formed by the S^{2-} anions. The conventional description of an fcc array has four ions located at the 4(a) positions 0, 0, 0; 0, $\frac{1}{2}$, $\frac{1}{2}$; $\frac{1}{2}$, 0, $\frac{1}{2}$ and $\frac{1}{2}$, $\frac{1}{2}$, 0 within a unit cell of symmetry $Fm\bar{3}m$. There are $2 \times 2 \times 2$ unit cells of this type within the idealized unit cell of $Ag_4Sn_3S_8$, such that the fcc sublattice is formed by $32 \times S^{2-}$. Within the published space group of $P4_132$ [19], these comprise two symmetry independent sites: S1 in the general 24(e) positions at x, y, z etc with $x_{S1} = \frac{1}{8}$ and $y_{S1} = z_{S1} = \frac{7}{8}$ and S2 in the 8(c) positions at x, x, x etc with $x_{S2} = \frac{1}{8}$. Both the S1 and S2 sites have $9 \times$ S1 and $3 \times$ S2 ions as nearest neighbours.

As discussed in section 1, an fcc structured anion sublattice contains one octahedral (O) and two tetrahedral (T) interstices per anion. Within the $P4_132$ description of $Ag_4Sn_3S_8$, the $32 \times O$ and $64 \times T$ positions each comprise four symmetry independent sets of sites. These positions are labelled $O1$–$O4$ and $T1$–$T4$. Their crystallographic descriptions are given in table 1 and their locations within the idealized unit cell are illustrated in figure 2. Each O centred octahedron shares eight faces with T centred tetrahedra and 12 edges with other octahedra, whilst each T centred tetrahedron shares four faces with O centred octahedra and six edges with other tetrahedra. The interconnectivity between the various polyhedra is described in table 1. Its significance will become clear later when describing the Ag^+ conduction mechanisms within $Ag_4Sn_3S_8$ at elevated temperatures.

3.3. Neutron diffraction measurements

Initial refinements of the powder neutron diffraction data collected at $T = 297(1)$ K were performed using the structural description reported by Amiel *et al* for $Ag_{3.8}Sn_4S_8$ [19], with the slightly distorted fcc structured anion sublattice formed by the two sets of S^{2-} positions described above and the Sn^{4+} located in the $O4$ interstices. In their work, four of the $15.2 \times Ag^+$

Table 1. Crystallographic descriptions of the various octahedral (O) and tetrahedral (T) cavities within an fcc anion sublattice formed by $32 \times S^{2-}$ located on the S1 and S2 sites within space group $P4_132$.

Label	Site	Position	Vertices	Shared faces	Shared edges
$O1$	4(a)	$\frac{3}{8}, \frac{3}{8}, \frac{3}{8}$ etc	$6 \times$ S1	$2 \times T2 + 6 \times T4$	$3 \times O2 + 6 \times O3 + 3 \times O4$
$O2$	4(b)	$\frac{7}{8}, \frac{7}{8}, \frac{7}{8}$ etc	$6 \times$ S1	$2 \times T1 + 6 \times T4$	$3 \times O1 + 3 \times O3 + 6 \times O4$
$O3$	12(d)	$\frac{1}{8}, y, \frac{1}{4} + y$ with $y = \frac{1}{8}$ etc	$4 \times$ S1 + $2 \times$ S2	$2 \times T2 + 4 \times T3 + 2 \times T4$	$2 \times O1 + 1 \times O2 + 4 \times O3 + 5 \times O4$
$O4$	12(d)	$\frac{1}{8}, y, \frac{1}{4} + y$ with $y = \frac{7}{8}$ etc	$4 \times$ S1 + $2 \times$ S2	$2 \times T1 + 4 \times T3 + 2 \times T4$	$1 \times O1 + 2 \times O2 + 5 \times O3 + 4 \times O4$
$T1$	8(c)	x, x, x with $x = 0$ etc	$3 \times$ S1 + $1 \times$ S2	$1 \times O2 + 3 \times O4$	$3 \times T3 + 3 \times T4$
$T2$	8(c)	x, x, x with $x = \frac{1}{2}$ etc	$3 \times$ S1 + $1 \times$ S2	$1 \times O1 + 3 \times O3$	$3 \times T3 + 3 \times T4$
$T3$	24(e)	x, y, z with $x = 0$, $y = 0$, $z = \frac{1}{4}$ etc	$2 \times$ S1 + $2 \times$ S2	$2 \times O3 + 2 \times O4$	$1 \times T1 + 1 \times T2 + 3 \times T3 + 1 \times T4$
$T4$	24(e)	x, y, z with $x = 0$, $y = 0$, $z = \frac{3}{4}$ etc	$4 \times$ S1	$1 \times O1 + 1 \times O2 + 1 \times O3 + 1 \times O4$	$1 \times T1 + 1 \times T2 + 1 \times T3 + 3 \times T4$

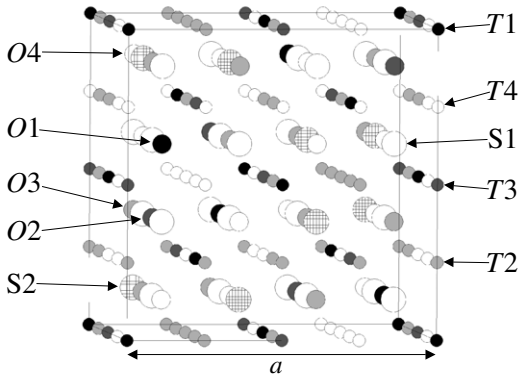

Figure 2. A schematic diagram showing an fcc structured sublattice of 32 sulfur anions formed by the S1 and S2 sites within space group $P4_132$ (largest spheres). The locations of the various octahedral (O) and tetrahedral (T) cavities within this fcc array are illustrated by the medium and smallest spheres, respectively (see table 1). The cubic lattice parameter a is also illustrated.

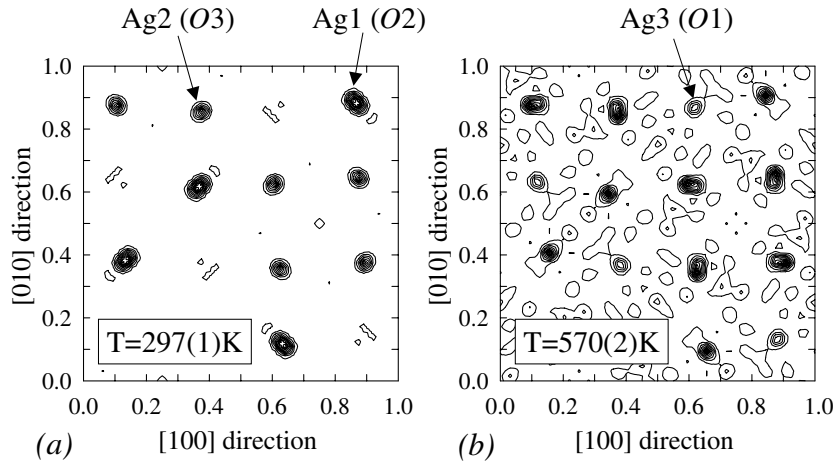

Figure 3. The time-averaged density of Ag^+ within the unit cell of $Ag_4Sn_3S_8$ at (*a*) $T = 297(1)$ and (*b*) $T = 570(2)$ K, projected down the [001] direction. The Ag^+ fully occupy the Ag1 and Ag2 positions at temperatures close to ambient, with an increasing fraction residing on the Ag3 sites at elevated temperatures.

per unit cell fill the $O2$ positions and the remainder are equally distributed over two partially occupied sets of 12-fold positions which are displaced from the $O3$ sites. This model, with $16 \times Ag^+$ per unit cell and using the previously published values of the positional and thermal vibration parameters [19], provided a relatively good fit to the data ($R_{WP} = 2.51\%$). However, attempts to vary several of these parameters led to a degree of instability within the least squares procedure, particularly for those variables associated with the two fractionally occupied Ag^+ sites. As a consequence, a more general approach was adopted in which the S^{2-} and Sn^{4+} positions are considered the 'known' structural fragments and maximum entropy Fourier difference methods are used to generate a map of the 'unknown' distribution of Ag^+ [27].

The resultant Ag^+ density within the unit cell at $T = 297(1)$ K is illustrated in figure 3(*a*) and shows that all 16 of these cations are located very close to the $O2$ and $O3$ octahedral sites.

The two cation positions are labelled Ag1 and Ag2, respectively, where the former corresponds to the Ag1 sites reported by Amiel *et al* [19]. Figure 3(*a*) indicates that the thermal vibrations of the cations are rather anisotropic but provides no evidence for Ag^+ at either the $O1$ sites or any of the tetrahedrally coordinated positions $T1$–$T4$. The Ag1 ($O2$) and Ag2 ($O3$) positions are fully occupied, because the total number of occupied sites ($4 \times O2$ plus $12 \times O3$) equals the population of $16 \times Ag^+$ within the unit cell[5].

The structural model of $Ag_4Sn_3S_8$ with the Sn, Ag1 and Ag2 filling, respectively, the $O4$, $O2$ and $O3$ interstices of the slightly distorted fcc sublattice formed by the S1 and S2 anions was used as the starting model for refinements of the powder neutron diffraction data. A relatively good fit ($R_{WP} = 2.44\%$) was obtained with the thermal vibrations constrained to be isotropic. However, allowing the Ag1 and Ag2 cations to vibrate anisotropically gave a significant improvement to $R_{WP} = 2.00\%$. Allowing the S1, S2 and Sn species to vary anisotropically, or permitting the Ag^+ to occupy the $O4$ or $T1$–$T4$ sites, produced no further meaningful reduction in R_{WP}. Thus, the final refinements used a total of 34 variables, comprising a scale parameter, 15 coefficients of a polynomial function describing the background level, two peak width parameters (Gaussian and Lorentzian components), the cubic lattice parameter a, six positional parameters (y_{Ag2}, y_{Sn}, x_{S1}, y_{S1}, z_{S1} and x_{S2}), three isotropic thermal vibration parameters (B_{iso} for S1, S2 and Sn) and six anisotropic thermal vibration parameters (B_{11} and B_{12} for Ag1 and B_{11}, B_{22}, B_{12} and B_{23} for Ag2). The fitted parameters are listed in table 2 and the quality of the fit illustrated in figure 4(*a*). The resultant crystal structure is shown in figure 5.

The structural parameters determined at ambient temperature were used as the starting model for the analysis of the neutron diffraction data collected at $T = 318(3)$ K and this procedure followed in an iterative manner to determine the evolution of the structure of $Ag_4Sn_3S_8$ with temperature up to $T = 570(2)$ K. At the highest temperatures a small, but significant, reduction in the quality of the fits was observed. A repeat of the maximum entropy Fourier difference procedure used at ambient temperature to determine the Ag^+ distribution within the unit cell (figure 3(*a*)) using the powder neutron diffraction data collected at $T = 570(2)$ K indicated the presence of a small, but significant, cation density at the $O1$ positions (see figure 3(*b*)). As a result, the refinement of the diffraction data collected at the highest temperature included the possibility of additional Ag3 cations at the $O1$ sites. The $O1$ positions contain no variable positional parameters (see table 1), so the addition of the Ag3 cations effectively results in a further three variable parameters, comprising the fractional site occupancies m_{Ag1}, m_{Ag2} and m_{Ag3}, (but with the constraint of the overall stoichiometry, i.e. $n_{Ag1} + n_{Ag2} + n_{Ag3} = 16$, where the n_i denote the population of Ag^+ on site i within the unit cell and are obtained by multiplying the fractional site occupancies m_i by their respective site multiplicities) and an isotropic thermal vibration parameter for the Ag3 cations. Allowing the Ag3 cations to vibrate anisotropically about the mean positions provided no improvement in the quality of the fit. The resultant fitted parameters are listed in table 2 and the quality of the fit illustrated in figure 4(*b*). Significantly, the increasing population of Ag3 cations occurs at the expense of the Ag2 ones, with the full occupancy of the $O2$ sites by Ag1 cations retained up to the maximum temperature measured ($T = 570(2)$ K).

Attempts to fit the diffraction data collected at intermediate temperatures using the structural model including the Ag3 cations showed no significant occupancy of these positions at temperatures below 500 K (see figure 6). As a result, the temperature dependences of the structural parameters presented in table 3 and illustrated in figures 7–9 were obtained with the Ag3 cations only included in the refinements of the data collected at the three

[5] The stoichiometry of the sample was confirmed to be $Ag_4Sn_3S_8$ by later refinements of the powder neutron diffraction data allowing the overall Ag^+ content to vary, which gave no significant improvement to the quality of the fit.

Table 2. Summary of the structural properties of $Ag_4Sn_3S_8$ determined by Rietveld refinement of the powder neutron diffraction data collected at $T = 297(1)$ K and $T = 570(2)$ K. The B_{ij} are the components of the anisotropic thermal vibrations (defined by $B_{ij} = 8\pi^2\langle u_{ij}^2\rangle$, where u_{ij} is the mean square amplitude of the vibration in direction ij) and B_{iso} is the isotropic thermal vibration parameter. The fractional site occupancies m are used to give the number n of Ag^+ occupying that site. The symbol * indicates that the value given is fixed during the refinements. N_D, N_P and N_V are the numbers of data points, Bragg peaks and variables used in the refinements, respectively, and the profile (P), weighted profile (WP) and expected (EXP) R-factors are defined in section 2.

T (K)		297(1)	570(2)
a (Å)		10.808 98(7)	10.8901(1)
V/Z (Å^3)		157.8571(10)	161.438(2)
Ag1	B_{11} (=B_{22}=B_{33}) (Å^2)	2.51(9)	5.5(3)
($O2$ in 4(b) at	B_{12} (=B_{23}=B_{13}) (Å^2)	−1.11(8)	−1.3(3)
$\frac{7}{8}, \frac{7}{8}, \frac{7}{8}$ etc)	m	1*	1.01(3)
	n	4*	4.04(12)
Ag2	y	0.145 25(17)	0.1443(4)
($O3$ in 12(d) at	B_{11} (Å^2)	1.71(14)	7.6(6)
$\frac{1}{8}, y, \frac{1}{4} + y$ etc)	B_{22} (=B_{33}) (Å^2)	2.66(6)	7.1(2)
	B_{12} (=−B_{13}) (Å^2)	1.16(6)	4.7(3)
	B_{23} (Å^2)	−0.09(9)	−1.5(4)
	m	1*	0.89(4)
	n	12*	10.7(5)
Ag3	B_{iso} (Å^2)	—	12(2)
($O1$ in 4(a) at	m	0*	0.32(6)
$\frac{3}{8}, \frac{3}{8}, \frac{3}{8}$ etc)	n	0*	1.3(2)
Sn	y	0.885 53(12)	0.8859(2)
($O4$ in 12(d) at	B_{iso} (Å^2)	0.75(2)	1.52(5)
$\frac{1}{8}, y, \frac{1}{4} + y$ etc)			
S1	x	0.1379(3)	0.1356(8)
(24(e) at x, y, z etc)	y	0.8904(3)	0.8914(8)
	z	0.9004(3)	0.9002(6)
	B_{iso} (Å^2)	0.85(3)	2.16(10)
S2	x (=y=z)	0.1278(3)	0.1250(6)
(8(c) at x, x, x etc)	B_{iso} (Å^2)	0.71(5)	2.15(16)
N_D		3755	3754
N_P		452	459
N_V		34	37
R_P		3.40	1.20
R_{WP}		2.00	0.70
R_{EXP}		0.83	0.38

highest temperatures. Of particular interest is the noticeable downward curvature of the lattice parameter a (figure 7) and the increasing anisotropy of the thermal vibrations of both the Ag1 (figure 8) and Ag2 (figure 9) cations with increasing temperature.

3.4. Molecular dynamics simulations

The validity of the computer simulations using the interionic potentials described in section 2 is confirmed by the stability of the simulated crystal structure of $Ag_4Sn_3S_8$ under ambient conditions and by the agreement between the calculated mean ionic positions at 300 K

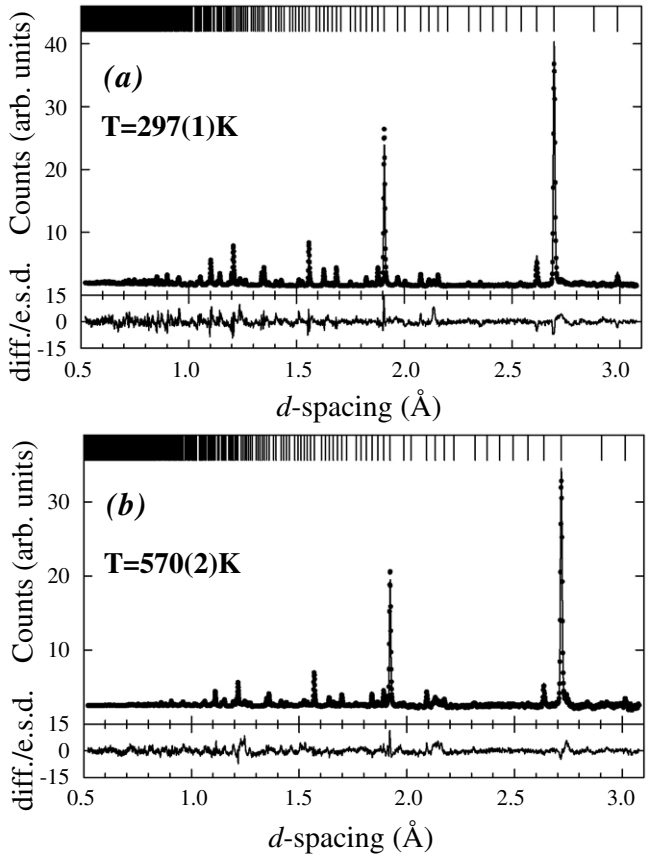

Figure 4. The least squares fit to the powder neutron diffraction data collected from $Ag_4Sn_3S_8$ at (*a*) $T = 297(1)$ K and (*b*) $T = 570(2)$ K. The dots are the experimental data points and the solid curve is the profile calculated using the parameters listed in table 2. The lower trace shows the difference (measured minus calculated) divided by the estimated standard deviation on the experimental data points. The row of tick marks along the top of the figure denote the calculated positions of all the Bragg reflections allowed by $P4_132$ symmetry.

($y_{Ag2} = 0.150$, $y_{Sn} = 0.880$, $x_{S1} = 0.133$, $y_{S1} = 0.893$, $z_{S1} = 0.903$ and $x_{S2} = 0.120$) and the experimentally derived values at $T = 297(1)$ K (see table 2). Further support is given by the onset of Ag^+ disorder, demonstrated by an increased number of Ag3 cations occupying the $O1$ sites within the simulations at temperatures greater than 500 K (figure 6). As in the powder neutron diffraction case (section 3.3), the latter occurs via the reduction in the number of Ag2 cations on the $O3$ sites (rather than the Ag1 cations on the $O2$ sites). However, at temperatures in excess of 600 K there is also a reduction in the population of the Ag1 cations and, as the temperature is increased further, the simulated system reaches a time-averaged state in which the $16 \times Ag^+$ per unit cell are equally distributed over all 20 of the available octahedrally coordinated sites ($4 \times O1 + 4 \times O2 + 12 \times O3$), such that the populations of the Ag1, Ag2 and Ag3 sites approach $\frac{16}{5}$, $\frac{48}{5}$ and $\frac{16}{5}$, respectively.

The site occupancies derived from the simulations shown in figure 6 were determined using the polyhedral analysis method used previously [41, 42]. At each time step the simulation box is divided into the various polyhedra (centred on the $O1$–$O4$ and $T1$–$T4$ sites) formed by the instantaneous positions of the individual S1 and S2 anions which form their vertices.

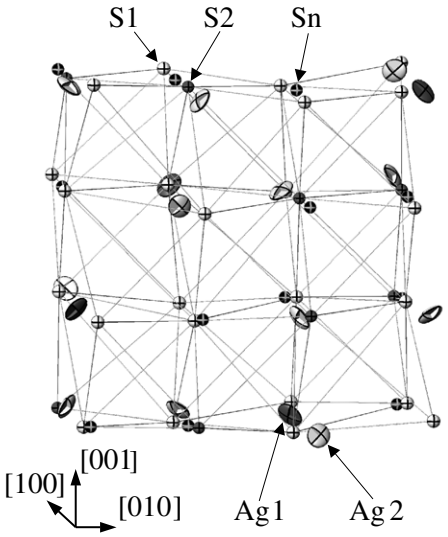

Figure 5. The crystal structure of $Ag_4Sn_3S_8$ determined by Rietveld refinements of powder neutron diffraction data collected at $T = 297(1)$ K and showing the anisotropic thermal vibrations of the Ag^+ located at the Ag1 and Ag2 positions. The narrow lines linking the various nearest neighbour S1 and S2 ions illustrate the distortion of the fcc anion sublattice.

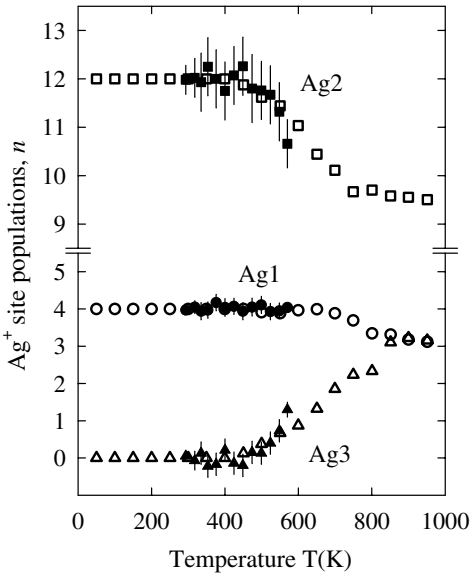

Figure 6. The temperature dependence of the measured occupancies of the three Ag^+ sites Ag1 (●), Ag2 (■) and Ag3 (▲), illustrating the increasing population of the latter at temperatures in excess of ≈500 K. The corresponding values provided by the polyhedral analysis of the computer simulations (see section 3.4) are shown as open symbols.

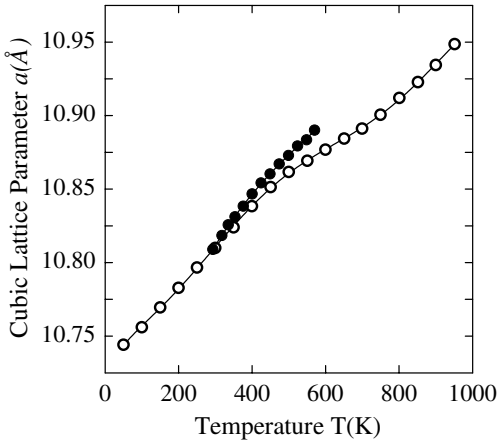

Figure 7. The temperature dependence of the measured cubic lattice parameter a of $Ag_4Sn_3S_8$ (●). The corresponding values provided by the computer simulations are shown as open symbols. The solid curves are guides to the eye.

This process completely fills all the available space. Each Ag^+ cation is then assigned to lie inside one of these polyhedra and, after averaging over all time steps and all cations, the average occupancy of the various O and T sites are obtained. As noted previously [43], care must be taken when using this approach, since the (simulated) fraction of cations within each polyhedron cannot be directly compared with the (measured) occupancy of the sites at the centre of these polyhedra. Nevertheless, the advantages of this method in providing a straightforward approach for visualizing the ionic conduction process generally outweighs such reservations (see, for example, [10, 41, 42]).

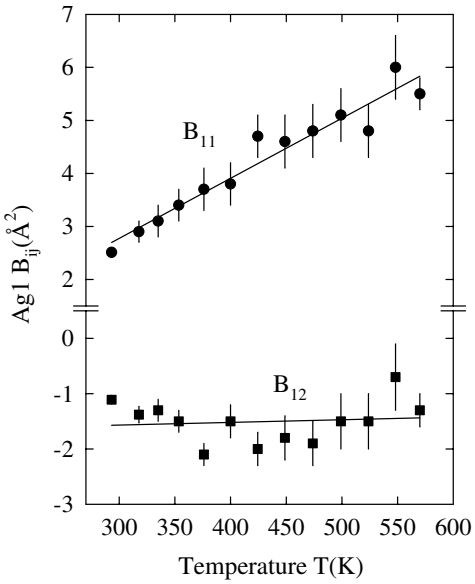

Figure 8. The temperature dependence of the anisotropic thermal vibration parameters B_{11} (●) and B_{12} (■) of the Ag1 cations. The solid lines are guides to the eye.

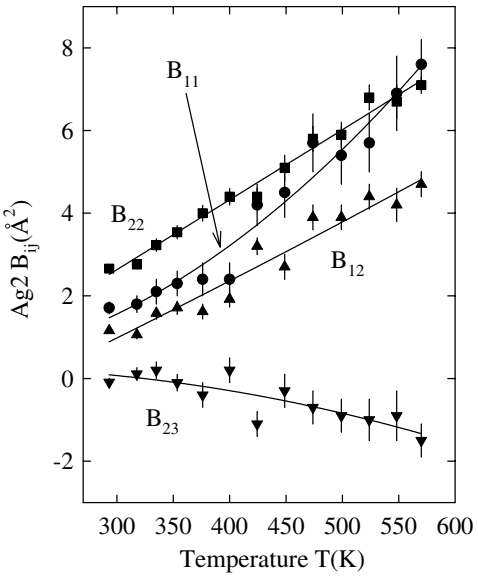

Figure 9. The temperature dependence of the anisotropic thermal vibration parameters B_{11} (●), B_{22} (■), B_{12} (▲) and B_{23} (▼) of the Ag2 cations. The solid lines are guides to the eye.

Table 3. The temperature dependence of selected structural parameters of $Ag_4Sn_3S_8$ determined by Rietveld refinement of the powder neutron diffraction data. To avoid unnecessary duplication, the values obtained at the lowest ($T = 297(1)$ K) and highest ($T = 570(2)$ K) temperatures given in table 2 are not included. The behaviour of the anisotropic thermal parameters of the Ag1 and Ag2 cations on increasing temperature is shown in figures 8 and 9.

		Sn		S1				S2	
	Ag2								
T (K)	y	y	B_{iso} (Å^2)	x	y	z	B_{iso} (Å^2)	x (=$y = z$)	B_{iso} (Å^2)
318(3)	0.1457(3)	0.8865(2)	0.84(3)	0.1374(5)	0.8909(5)	0.9001(5)	0.99(6)	0.1284(5)	0.83(10)
335(2)	0.1458(4)	0.8864(3)	0.90(5)	0.1368(8)	0.8907(7)	0.8999(6)	1.12(9)	0.1283(7)	1.13(15)
353(2)	0.1459(4)	0.8859(3)	0.96(5)	0.1372(8)	0.8910(7)	0.8997(7)	1.18(9)	0.1282(6)	1.10(15)
376(2)	0.1453(5)	0.8862(3)	0.91(5)	0.1369(9)	0.8913(8)	0.8991(8)	1.45(10)	0.1280(7)	1.22(16)
400(2)	0.1462(5)	0.8862(3)	1.03(5)	0.1363(9)	0.8921(8)	0.9002(8)	1.38(10)	0.1265(8)	1.43(18)
424(2)	0.1450(5)	0.8857(3)	1.14(6)	0.1345(9)	0.8912(8)	0.9008(7)	1.46(11)	0.1261(8)	1.68(19)
449(2)	0.1447(6)	0.8868(3)	1.09(6)	0.1353(10)	0.8924(9)	0.8985(9)	1.65(13)	0.1260(9)	2.0(2)
474(2)	0.1440(6)	0.8862(4)	1.23(6)	0.1360(11)	0.8917(9)	0.8997(9)	1.83(14)	0.1270(9)	2.0(2)
499(2)	0.1451(6)	0.8859(4)	1.28(6)	0.1354(11)	0.8921(9)	0.9002(9)	1.80(14)	0.1247(10)	2.1(2)
524(2)	0.1442(7)	0.8865(4)	1.45(7)	0.1348(13)	0.8933(10)	0.8994(10)	2.05(16)	0.1249(10)	1.9(2)
548(2)	0.1446(7)	0.8866(4)	1.36(7)	0.1356(14)	0.8916(12)	0.8982(11)	2.50(19)	0.1261(11)	2.4(3)

In the case of $Ag_4Sn_3S_8$, analysis of the simulated trajectories of the Ag^+ through the slightly distorted fcc sublattice of S^{2-} indicate that two conduction pathways are favoured. At the onset of thermally induced cation disorder at $T \sim 500$ K the predominant hopping mechanism involves motion of Ag^+ between the $O3$ (Ag2) and $O1$ (Ag3) positions via the tetrahedrally coordinated $T2$ sites. An example of this motion is illustrated in figure 10. The simulations at temperatures in excess of 600 K indicate that the Ag1 cations located in the $O2$ positions also undergo diffusion to the 'empty' $O1$ sites, in this case via the $T4$

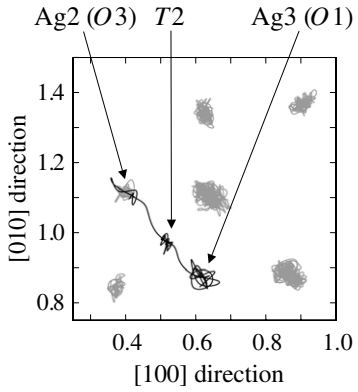

Figure 10. A section through a portion of the MD simulations of $Ag_4Sn_3S_8$ at $T = 500$ K viewed down the [001] direction. The trajectories of a single Ag^+ ion undergoing diffusion from the $O2$ to the 'empty' $O1$ sites via the $T2$ interstices is shown by the black trace. For clarity, other neighbouring Ag^+ ions are shown in grey and the Sn^{4+} and S^{2-} trajectories are not illustrated.

tetrahedral interstices. At the highest temperatures extensive disorder is observed, with all the Ag^+ involved in the conduction process. However, the majority of the hops can still be identified as either $O3 \leftrightarrow T2 \leftrightarrow O1$ or $O2 \leftrightarrow T4 \leftrightarrow O1$ processes, though the presence of a significant fraction of vacancies on the $O2$ and $O3$ sites allows some direct hops between these positions to occur, corresponding to the transfer of Ag1 and Ag2 cations. This pathway is via the $T4$ sites, because $T4$ centred tetrahedra share a common face with both $O2$ and $O3$ centred octahedra (see table 1).

No evidence of diffusion of Sn^{4+} within the simulations was observed at any temperature up to the melting point of the simulated configuration, which occurred during the calculations at 1000 K. Taking into account the need for superheating to achieve melting within MD simulations, this value is in excellent agreement with the experimental value of 941 K [22].

4. Discussion

As discussed in section 3.3, the crystal structure adopted by $Ag_4Sn_3S_8$ under ambient conditions consists of an ordered distribution of the $16 \times Ag^+$ and $12 \times Sn^{4+}$ per unit cell over the 32 octahedrally coordinated interstices formed by a slightly distorted fcc structured sublattice of S^{2-}. This ionic arrangement can, to a good approximation, be described as a cation deficient rock-salt structure and is in broad agreement with the structure of $Ag_{3.8}Sn_3S_8$ previously reported by Amiel *et al* [19]. An exception is that the neutron diffraction results presented here show the Ag^+ to be distributed over two symmetry independent, and fully occupied, sets of positions at ambient temperature, rather than three sites (two of which are only partially occupied [19]).

The refined positional parameters for $Ag_4Sn_3S_8$ at $T = 297(1)$ K listed in table 2 indicate that the two symmetry independent sets of sites which form the anion sublattice, S1 and S2, are displaced away from the 'ideal' positions required to generate a undistorted fcc array by $\approx$0.35 and $\approx$0.05 Å, respectively. As a consequence, the 12 nearest neighbour anions around the S1 positions comprise $9 \times$ S1 and $3 \times$ S2 at a total of nine different distances in the range 3.555(4)–4.419(5) Å (average = 3.871(4) Å), with the $24 \times$ S–S1–S angles taking a total of 21 different values in the range 49.55(1)–68.63(1)° which span the 'ideal' value of 60°. The environment around the S2 positions is rather more regular, with $3 \times$ S1 at each of three

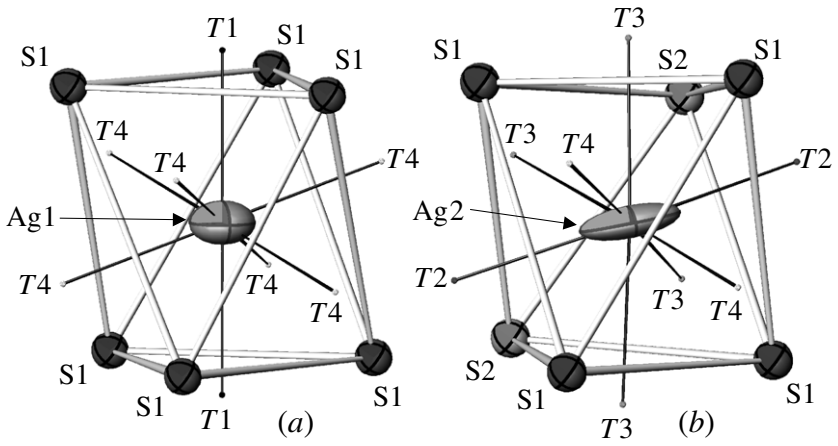

Figure 11. The Ag^+ thermal ellipsoids demonstrating the highly anisotropic thermal vibrations of (*a*) the Ag1 and (*b*) the Ag2 cations within their anion octahedra at $T = 570(2)$ K. The ionic densities extend preferentially towards the neighbouring $T4$ and $T2$ positions, respectively.

distances 3.555(4), 3.614(4) and 3.890(4) Å, plus $3 \times$ S2 at 3.822(4) Å (average = 3.720(4) Å), giving S–S2–S angles in the range 55.88(1)°–65.05(1)°.

The distortion of the anion sublattice also has the effect of modifying the sizes of the various octahedral (O) and tetrahedral (T) interstices and slightly displacing their centres away from the ideal locations given in table 1. The Sn^{4+} are located in the smallest set of octahedral interstices (the $O4$ sites) and the distortion of the fcc sublattice can thus be viewed as a means of simultaneously accommodating both the Ag^+ ($r_{Ag^+} = 1.15$ Å [39]) and the smaller Sn^{4+} cations ($r_{Sn^{4+}} = 0.69$ Å [39]) within octahedral environments. The Sn^{4+} are surrounded by $2 \times$ S1 at 2.541(3) Å, $2 \times$ S1 at 2.546(2) Å and $2 \times$ S2 at 2.620(3) Å, giving an average Sn^{4+}–S^{2-} distance of 2.569(2) Å and S^{2-}–Sn^{4+}–S^{2-} angles in the range 86.95(1)°–93.66(1)°. The former is in good agreement with the value of 2.572 Å observed within octahedrally coordinated SnS_2 [44]. The octahedral coordination surrounding the Ag1 and Ag2 cations is rather more distorted than that around the Sn^{4+}. The Ag1 cations have $6 \times$ S1 at a distance of 2.860(3) Å and S1–Ag1–S1 angles of 80.86(1)° ($\times 6$), 97.18(1)° ($\times 3$) and 101.20° ($\times 3$), whilst the Ag2 cations are surrounded by $2 \times$ S1 at 2.592(3) Å, $2 \times$ S1 at 2.786(3) Å and $2 \times$ S2 at 2.897(3) Å (average = 2.758 Å) and have seven different S–Ag2–S angles in the range 82.15(1)°–104.96(1)°.

On increasing temperature there is relatively little change in the structure of the fcc sublattice (see table 3) and the extent of the distortion away from its ideal configuration remains significant up to the highest temperature measured ($T = 570(2)$ K). Experimentally, the most significant changes observed on increasing temperature are the increasing anisotropy in the thermal vibrations of both the Ag1 and Ag2 cations (see figures 8 and 9) and the increasing occupancy of the 'empty' $O1$ sites by Ag3 cations at temperatures in excess of ≈500 K (figure 6). The extents of the former displacements at $T = 570(2)$ K are illustrated in figure 11. The thermal ellipsoids of the Ag2 cations (figure 11(*b*)) are elongated towards two of the eight triangular faces of their surrounding octahedra and, specifically, extend preferentially towards the neighbouring two $T2$ positions. The anisotropy in the thermal vibrations of the Ag1 cations is slightly less pronounced, with the ellipsoids flattened perpendicular to the two faces shared with $T1$ centred tetrahedra and extending towards the other six faces which are common to $T4$ centred tetrahedra.

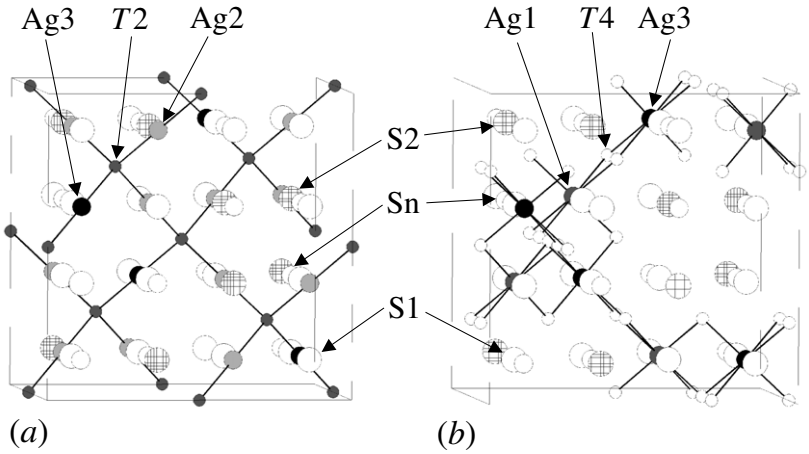

Figure 12. The network of conduction pathways formed (*a*) by hops of Ag2 ($O3$) cations to form Ag3 ($O1$) cations via the $T4$ sites and (*b*) by hops of Ag1 ($O2$) cations to form Ag3 ($O1$) cations via the $T2$ sites.

The experimentally determined anisotropy in the thermal vibrations of the Ag1 and Ag2 cations discussed above is entirely consistent with the diffusion pathways observed within the MD simulations, in which diffusion to the 'empty' $O1$ (Ag3) sites occurs via the $T4$ and $T2$ positions, respectively. The greater anisotropy of the measured thermal vibrations of the Ag2 cations also supports the observation that the onset of dynamic Ag^+ disorder occurs within the simulations in two stages, with the Ag2 cations contributing to the ionic transport at slightly lower temperatures than the Ag1 ones. Unfortunately, it was not possible to confirm the latter process during the diffraction experiments, owing to degradation of the sample at temperatures in excess of ∼600 K.

The two Ag^+ diffusion mechanisms ($O3$(Ag2) $\leftrightarrow$ $T2$ $\leftrightarrow$ $O1$(Ag3) and $O2$ (Ag1)$\leftrightarrow$ $T4$ $\leftrightarrow$ $O1$(Ag3)) are illustrated in figure 12. Both form long range pathways through the lattice and comprise individual hops in $\langle 111 \rangle$ directions of a distance of $\approx\sqrt{3}a/8 \approx 2.4$ Å. The two sets of pathways meet at the $O1$ positions and, as observed within the simulations at temperatures in excess of 600 K, the Ag^+ readily transfer between the two routes. There is no evidence of direct hops between the various octahedra via shared edges. Within the model of Ag^+ diffusion between octahedrally coordinated sites via the tetrahedral interstices, the observed preference for hopping via the $T2$ and $T4$ sites is clear from table 1. The $T2$ centred tetrahedra exclusively share common faces with both $O3$ (Ag2) and $O1$ (Ag3) centred units, whilst the $T4$ centred polyhedra are the only ones which share common faces with both $O2$ (Ag1) and $O1$ (Ag3) centred octahedra. The onset of the former mechanism at a slightly lower temperatures could be a consequence of Coulomb repulsion effects, since the $T4$ centred polyhedra share a common face with a single $O4$ centred unit (which contain the Sn^{4+}) and may represent a slightly higher energy barrier to diffusion than the $T2$ centred ones which do not. On these grounds, occupancy of the $T3$ and $T1$ centred tetrahedra, which share two and three faces with $O4$ centred octahedra, respectively (see table 1), would not be energetically favourable. This is supported by the MD simulations, which show no significant occupancy of these two positions at any temperature.

The onset of thermally induced Ag^+ disorder within $Ag_4Sn_3S_8$ is promoted by the availability of the empty $O1$ cavities. However, at the highest temperatures the time-averaged distribution of Ag^+ within the simulations approximates to an equal occupancy of $\frac{4}{5}$ for all the

$O1$, $O2$ and $O3$ sites. This highly disordered arrangement is stable within the simulations from ∼700 K to the melting point of 1000 K and corresponds to a levelling off in the curve of ionic conductivity versus temperature (figure 1). A detailed comparison between the experimental and simulated conductivities is made difficult by the uncertainties in both approaches discussed in section 3.1 and by the limited temperature range over which the data overlap[6]. At lower temperatures the simulations give no conductivity information because no Ag^+ diffusion occurs within the timescale of the calculations, whilst degradation of the sample places an upper limit on the temperature range which can be accessed experimentally. Nevertheless, the latter clearly show a steep rise in the temperature region at which significant Ag^+ disorder is observed within both simulations and the neutron diffraction studies (figure 6) and also provide some evidence for a slower rate of increase at temperatures above ∼500 K (see figure 1). The latter is typical of superionic compounds which undergo gradual transitions to the highly conducting state (for a recent review, see [1]) and generally interpreted in terms of increased correlations between the motions of diffusing ions. In the case of Ag^+ containing superionics, such correlations are observed experimentally in, for example, the low values of Haven's ratio [40] and the presence of diffuse x-ray scattering [45].

The continuous increase in ionic conductivity and the absence of any symmetry change with increasing temperature demonstrate that $Ag_4Sn_3S_8$ undergoes a type-II superionic transition at ≈500 K (in the notation of Boyce and Huberman [2]). This contrasts with the type-I behaviour of the parent material Ag_2S, which has a first-order phase transition at 452 K from the fully ordered β phase (space group $P2_1/c$ [46]) to the superionic α phase in which the cations are disordered predominantly over the tetrahedrally coordinated interstices within a bcc structured anion sublattice (space group $Im\bar{3}m$ [45, 47]). In addition to the rapid, though continuous, increase in the ionic conductivity with temperature, the presence of a type-II superionic transition is often associated with anomalies in the specific heat capacity, elastic constants and lattice expansivity (see [1], and references therein). For the latter, increases in $\mathrm{d}a/\mathrm{d}T$ are observed at temperatures close to the onset of superionic behaviour within, for example, β-PbF_2 [48], Li_2O [49] and the high pressure rock-salt structured form of AgI [11]. In this context, the *decrease* in $\mathrm{d}a/\mathrm{d}T$ observed experimentally in $Ag_4Sn_3S_8$ and seen more dramatically within the MD simulations (figure 7) is rather surprising. A possible explanation is provided by the relative sizes of the various polyhedral cavities, because the $O1$ centred octahedra are somewhat larger than their $O2$ and $O3$ centred counterparts and Coulomb attractions due to the presence of Ag3 cations at the $O1$ sites would tend to reduce the lattice volume. Alternatively, as listed in table 1, the $O1$, $O2$ and $O3$ octahedra share edges with three, six and five of the $O4$ octahedra which contain Sn^{4+}, respectively. As a consequence, the transfer of Ag^+ to the 'empty' $O1$ sites reduces the number of the shortest Ag^+–Sn^{4+} contacts and may also facilitate a reduction in the lattice volume.

To assess the wider implications of the cation disorder within $Ag_4Sn_3S_8$ it is necessary to identify a compound possessing an fcc structured anion sublattice which undergoes a type-II superionic transition on heating. However, Ag^+ based superionics are more often characterized by type-I superionic transitions, as in the cases of Ag_2S at 452 K and AgI at 470 K (see [1]). The application of high pressure transforms AgI to a rock-salt structured modification (AgI-III) and this phase has been shown to undergo a continuous (type-II) superionic transition on heating [9, 36]. Neutron diffraction experiments and MD simulations conducted at elevated pressures and temperatures show that the onset of thermally induced disorder within AgI-III is characterized by an increasing occupancy of the tetrahedrally coordinated interstices [10, 11].

[6] The tendency of the interionic potentials to underestimate the thermal expansion of $Ag_4Sn_3S_8$ (see figure 7) will, in principle, also contribute to this discrepancy. However, simulations performed at various (fixed) volumes showed that the resultant changes in the ionic conductivity are relatively small in comparison to the differences shown in figure 1.

In $Fm\bar{3}m$ symmetry all the octahedrally (O) and all the tetrahedrally (T) coordinated interstices are identical and the reported $O \leftrightarrow T \leftrightarrow O$ diffusion mechanism within AgI-III is, therefore, analogous to that observed within $Ag_4Sn_3S_8$. However, MD simulations show that the residence times of the cations on the O and T sites are comparable within the disordered phase of AgI-III [10]. In the case of $Ag_4Sn_3S_8$, the diffusion between the various O sites occurs via the $T2$ and $T4$ positions, but the tetrahedrally coordinated sites are not stable energy minima for the Ag^+. In those cases where the Ag^+ are observed to remain in the T sites (such as the example illustrated in figure 10), the residence times are only a few picoseconds, and over an order of magnitude lower that the typical values for the octahedrally coordinated O positions.

5. Conclusions

The work presented in this paper forms the first part of a wider study of the structural and ionic conductivity behaviour of ternary chemical derivatives of Ag_2S. The role of added isovalent and aliovalent cation species in the halide counterpart AgI has been more extensively studied and a number of features have emerged. In general, the 'dopant' cations modify the structure of the I^- sublattice in order to accommodate their specific crystal chemical requirements and achieve a favoured anion coordination environment. This invariably requires the anion sublattice to be modified from the bcc arrangement characteristic of the superionic α-AgI phase, probably because the octahedrally and tetrahedrally coordinated interstices within a bcc array are both highly distorted and less able to accommodate the added cations' requirements for more symmetrical environments [8]. In the case of $RbAg_4I_5$, the larger size of the Rb^+ forces the anion sublattice to adopt a β-Mn-type arrangement [13], whilst phases such as α-Ag_2HgI_4, Ag_3SnI_5 and Ag_4PbI_6 possess fcc I^- arrays and the divalent cations occupy close to ideal coordination environments (tetrahedral in the former compound and octahedral in the other two) [5–8].

As discussed in section 1, an fcc structured sublattice is less conducive to high ionic conductivity than its bcc structured counterpart because the number of interstices available for diffusing Ag^+ is lower. This is, to some extent, compensated in the cases of α-Ag_2HgI_4, Ag_3SnI_5 and Ag_4PbI_6 by the presence of charge compensating vacancies on the cation sites and by the divalent species also being mobile [5–8]. The behaviour of $Ag_4Sn_3S_8$ broadly mirrors that of these AgI derivatives, with the bcc structure characteristic of Ag_2S in its lowest temperature superionic phase [45, 47] transformed into a (slightly distorted) fcc structured form to accommodate the Sn^{4+} and the extensive Ag^+ disorder observed at elevated temperatures is clearly facilitated by the presence of empty octahedrally coordinated sites at the $O1$ positions. However, there is no evidence of diffusion of Sn^{4+} within $Ag_4Sn_3S_8$, presumably due to prohibitively large Coulomb energies associated with the motion of such a highly charged species.

Finally, it is important to emphasize the need to employ a number of complementary techniques in order to provide an accurate and reliable description of the structural and diffusion behaviour of systems exhibiting thermally induced ionic disorder. In this case, the experimental data obtained by powder neutron diffraction and impedance spectroscopy techniques are essential for validating the results of the MD simulations, which are based on empirical potentials. Confidence in the latter then enables the results of the calculations to be interrogated to probe the motions of individual ion motions. In addition, it is possible to 'predict' the behaviour of compounds such as $Ag_4Sn_3S_8$ at temperatures which, for reasons of chemical stability, cannot reliably be accessed by experimental methods.

Acknowledgments

The authors are grateful to P A Madden and M Wilson for their assistance with the computer simulations presented in this paper and to D S Sivia for help in the preparation of the maximum

entropy Fourier maps. One of the authors (PB) wishes to acknowledge financial support provided by the Swedish Research Council.

References

[1] Hull S 2004 *Rep. Prog. Phys.* **67** 1233–314
[2] Boyce J B and Huberman B A 1979 *Phys. Rep.* **51** 189–265
[3] Boyce J B, Hayes T M and Mikkelsen J C Jr 1981 *Phys. Rev.* B **23** 2876–96
[4] Miyatani S 1981 *J. Phys. Soc. Japan* **50** 3415–8
[5] Hull S and Keen D A 2000 *J. Phys.: Condens. Matter* **12** 3751–65
[6] Hull S and Keen D A 2001 *J. Phys.: Condens. Matter* **13** 5597–610
[7] Hull S, Keen D A and Berastegui P 2002 *Solid State Ion.* **147** 97–106
[8] Hull S, Keen D A and Berastegui P 2002 *J. Phys.: Condens. Matter* **14** 13579–96
[9] Mellander B-E 1982 *Phys. Rev.* B **26** 5886–96
[10] Keen D A, Hull S, Berastegui P, Barnes A C, Crichton W A, Madden P A, Tucker M G and Wilson M 2003 *Phys. Rev.* B **68** 014117
[11] Keen D A, Hull S, Hayes W and Gardner N J G 1996 *Phys. Rev. Lett.* **77** 4914–7
[12] Hull S, Keen D A, Sivia D S and Berastegui P 2002 *J. Solid State Chem.* **165** 363–71
[13] Hull S and Berastegui P 2004 *J. Solid State Chem.* **177** 3157–74
[14] Kuhs W F, Nitsche R and Scheunemann K 1979 *Mater. Res. Bull.* **14** 241–8
[15] Hellstrom E E and Huggins R A 1980 *J. Solid State Chem.* **35** 207–14
[16] Wada H and Onoda M 1991 *J. Less Common Met.* **175** 209–17
[17] Wada H 1992 *J. Alloys Compounds* **178** 315–23
[18] Wada H, Ishii M, Onoda M, Tansho M and Sato A 1996 *Solid State Ion.* **86–88** 159–63
[19] Amiel O, Frankel D C and Wada H 1995 *J. Solid State Chem.* **116** 409–21
[20] Amiel O and Wada H 1995 *J. Solid State Chem.* **115** 112–9
[21] Moh G H and Klein D 1977 *Neues Jb. Miner. Abh.* **131** 33–5
[22] Wang N 1977 *Neues Jb. Miner. Abh.* **131** 35–7
[23] Hull S, Smith R I, David W I F, Hannon A C, Mayers J and Cywinski R 1992 *Physica* B **180/181** 1000–2
[24] David W I F, Ibberson R M and Matthewman J C 1992 *Rutherford Appleton Laboratory Internal Report* RAL-92-032
[25] Brown P J and Matthewman J C 1987 *Rutherford Appleton Laboratory Internal Report* RAL-87-010
[26] Wilson A J C (ed) 1995 *International Tables for Crystallography* volume C (Dordrecht: Kluwer)
[27] Sivia D S and David W I F 2001 *J. Phys. Chem. Solids* **62** 2119–27
[28] Hull S, Keen D A, Sivia D S, Madden P A and Wilson M 2002 *J. Phys.: Condens. Matter* **14** L9–17
[29] Vashishta P and Rahman A 1978 *Phys. Rev. Lett.* **40** 1337–40
[30] Parrinello M, Rahman A and Vashishta P 1983 *Phys. Rev. Lett.* **50** 1073–6
[31] Vashishta P, Ebbsjö I, Dejus R and Sköld K 1985 *J. Phys. C: Solid State Phys.* **18** L291–6
[32] Ebbsjö I, Vashishta P, Dejus R and Sköld K 1987 *J. Phys. C: Solid State Phys.* **20** L441–7
[33] Madden P A, O'Sullivan K F and Chiarotti G 1992 *Phys. Rev.* B **45** 10206–12
[34] Seok C and Oxtoby D W 1997 *Phys. Rev.* B **56** 11485–92
[35] Seok C and Oxtoby D W 1998 *Phys. Rev.* B **58** 5146–8
[36] Tallon J L 1988 *Phys. Rev.* B **38** 9069–79
[37] Rains C A, Ray J R and Vashishta P 1991 *Phys. Rev.* B **44** 9228–39
[38] Matsunaga S and Madden P A 2004 *J. Phys.: Condens. Matter* **16** 181–94
[39] Shannon R D 1976 *Acta Crystallogr.* **A 32** 751–67
[40] Kobayashi M 1990 *Solid State Ion.* **39** 121–49
[41] Ihata K and Okazaki H 1997 *J. Phys.: Condens. Matter* **9** 1477–92
[42] Castiglione M J, Wilson M, Madden P A and Grey C P 2001 *J. Phys.: Condens. Matter* **13** 51–66
[43] Chahid A and McGreevy R L 1998 *J. Phys.: Condens. Matter* **10** 2597–609
[44] Palosz B and Salje E 1989 *J. Appl. Crystallogr.* **22** 622–3
[45] Cava R J and McWhan D B 1980 *Phys. Rev. Lett.* **45** 2046–50
[46] Sadanaga R and Sueno S 1967 *Mineral J. Japan* **5** 124–43
[47] Cava R J, Reidinger F and Wuensch B J 1980 *J. Solid State Chem.* **31** 69–80
[48] Goff J P, Hayes W, Hull S and Hutchings M T 1991 *J. Phys.: Condens. Matter* **3** 3677–87
[49] Wilson M, Jahn S and Madden P A 2004 *J. Phys.: Condens. Matter* **16** S2795–810